On the merits of using multi-stage and counterflow electrodialysis for reduced energy consumption

On the merits of using multi-stage and counterflow electrodialysis for reduced energy consumption

Karim M. Chehayeb, Kishor G. Nayar, John H. Lienhard V*

Department of Mechanical Engineering, Massachusetts Institute of Technology, Cambridge, MA 02139, USA.

Abstract

The cost of electrodialysis (ED) systems can be decreased by decreasing their power consumption. Such reductions may be achieved by using degrees of freedom in the system's configuration to obtain a more uniform spatial distribution of the of rate entropy generation, as explained by the theorem of equipartition of entropy generation. In this paper, we study possible improvements to the energy efficiency of electrodialysis through the use of two electric stages with different voltages, and through operation in a counterflow configuration. We first consider how a two-stage ED system should be operated. In particular, we look at how the voltages and current densities should be chosen. In addition, we quantify the effect of operating under two voltages in brackish-water desalination and in high-salinity brine concentration. Finally, we quantify the effect of operating ED in counterflow for the same applications. We show that high ED fixed costs prevent the achievement of significant improvements in energy efficiency. If fixed costs are reduced, and larger systems become cost-effective, we show that a power reduction of up to 29% is possible by going from a single-stage to a two-stage configuration.

Keywords: equipartition of entropy generation, electrodialysis, brackish water desalination, brine concentration, energy efficiency

K.M. Chehayeb, K.G. Nayar, and J.H. Lienhard V, "On the merits of using multi-stage and counterflow electrodialysis for reduced energy consumption," *Desalination*, **439**:1-16, 1 August 2018.

*Corresponding author
Email address: lienhard@mit.edu (John H. Lienhard V)

Nomenclature

Acronyms

AEM	anion-exchange membrane
CEM	cation-exchange membrane

Symbols

A	effective cell-pair area [m^2]
a	activity [-]
C	cost [\$/m^3 product]
c^*	normalized cost [(\$/m^3 product)/(\$/kWh)]
c	concentration [mol/m^3]
D	diffusion coefficient of salt [m^2/s]
$Đ_{ij}$	Maxwell-Stefan diffusion coefficient for species i and j [m^2/s]
F	Faraday constant, 96,487 [C/mol]
f	driving force [J/mol-m-K]
h	channel height [m]
i	current density [A/m^2]
i	annual interest rate [-]
J	molar duty [mol/s]
j	molar flux [mol/m^2-s]
K_e	cost of electricity [\$/W-s]
K_m	fixed cost per unit cell-pair area per unit time [\$/m^2-s]
$K_\mathrm{m},0$	fixed cost per unit cell-pair area at time 0 [\$/m^2]
k_m	mass transfer coefficient [m/s]
L	phenomenological coefficient [K-mol^2/J-m-s]
L_s	salt permeability [m/s]
L_w	water permeability [mol/m^2-s-bar]
M	molar mass [g/mol]
m	molality [mol/kg]
P	power consumption [W]
R	universal gas constant, 8.3145 [J/mol-K]
Re	Reynolds number, Eq. D.4 [-]
r	electric resistance [Ω-m^2]
r	cost ratio, Eq. G.2 [W/m^2]
S	salinity [g/kg]
S	entropy [J/K]
$\dot{S}_\mathrm{gen}$	entropy generation rate [W/K]
$\dot{S}_\mathrm{gen,\ equip}$	entropy generation rate of the equivalent equipartitioned system [W/K]
$\dot{s}'''_\mathrm{gen}$	volumetric rate of entropy generation [W/m^3-K]
$\dot{s}''_\mathrm{gen}$	entropy generation rate per unit area [W/m^2-K]
Sc	Schmidt number, Eq. D.5 [-]
Sh	Sherwood number, Eq. D.1 [-]
T	absolute temperature [K]

T_s	salt transport number [-]
T_w	water transport number [-]
V	Volume [m^3]
V	voltage [V]
V_1^*	voltage of the first stage divided by that of the single-stage system [-]
$V_{1,P}^*$	normalized first-stage voltage that minimizes power consumption [-]
$V_{1,\mathrm{Var}(i)}^*$	normalized first-stage voltage that minimizes the variance of the current density [-]
$V_{1,\mathrm{Var}(\acute{s}_\mathrm{gen}'')}^*$	normalized first-stage voltage that minimizes the variance of rate of entropy generation [-]
W	stack width [m]
z	charge number

Greek

Δ	difference or change
δ	diffusion layer thickness [m]
∇	gradient
ε	spacer volume fraction [-]
Φ	electric potential [V]
$\gamma_\pm$	mean molal (or molar) activity coefficient [-]
μ	dynamic viscosity [Pa-s]
μ_i	electrochemical potential of ion i [J/mol]
μ_s	chemical potential of the salt [J/mol]
τ	plant life [years]
Ξ	equipartition factor [-]
ρ	density [$\mathrm{kg/m}^3$]

Subscripts

C	concentrate
cp	cell-pair
D	diluate
i	ion i
m	at membrane interface
s	salt
w	water

Superscripts

m	in membrane
s	in solution

1. Introduction

Electrodialysis (ED) is a desalination technology that can treat brackish water [1–8], seawater [9–13], and high-salinity brines [3, 14, 15], and has many applications in the food and beverage industry [3, 16].

The cost of ED can be decreased through the reduction of its power consumption. One way power consumption can be decreased is by increasing the system size[1]. The trade-off that exists between the costs related to the system size and the energy costs is well understood, and the choice of system size is determined through cost minimization, as was done in a previous study [17] for the use of ED for brackish-water desalination and high-salinity brine concentration.

1.1. Reducing energy consumption using the theorem of equipartition of entropy generation

A less commonly employed concept is that, for heat and mass transfer systems of fixed size, additional operation flexibility can also reduce power consumption. This can be explained by the theorem of equipartition of entropy generation, which was first introduced by Tondeur and Kvaalen [18]. This theorem states that, given a fixed duty (total quantity to be transported) and a fixed system size, the optimal configuration is that which minimizes the spatial or temporal variance in the rate of entropy generation. A more physical way of thinking about this concept is by considering the distribution of the available area. By better distributing the rate of entropy generation, the driving force is also better distributed (when flux is a linear function of the driving force), and more area is allocated to the part of the system where the driving force is higher. Thus, in a poorly equipartitioned system, part of the available area is wasted on sections where the driving force is very small, resulting in low fluxes.

1.2. Equipartition through the use of multiple stages and of counterflow operation

One way to achieve better equipartition of entropy generation is by operating the system under multiple stages. Staging results in additional degrees of freedom, which, even at a fixed system size, can lead to improvements in the system's energy efficiency. The idea of multi-staging has been previously applied to multiple desalination technologies such as humidification-dehumidification [19–22], membrane distillation [23], and reverse osmosis [24]. In the case of ED, each stage can be operated at a different voltage to better control the distribution of the flux. This is referred to in the literature as 'electric staging' of ED systems. In this paper, we use the term 'multi-staging' to exclusively imply 'electric staging', and use 'two stages' and 'two voltages' interchangeably.

Another way to better distribute the driving force over the available area is by operating a heat or mass exchanger in a counterflow configuration. In the case of ED, this can serve to better distribute the

[1] at least until a certain limit, as explained in Appendix A

concentration profiles over the length of the system, which might lead to improvements to the system's energy consumption.

Few studies have looked at the operation of ED under multiple voltages or in counterflow configurations. Tsiakis and Papageorgiou [25] modeled ED systems with multiple hydraulic and electric stages. The conditions at each stage were optimized numerically to minimize total system costs. Turek [9] studied a counterflow two-stage ED seawater desalination system and reported energy and cost numbers. Ryabtsev et al. [26] implemented a two-stage desalination system. The first stage was operated under a constant current density, and the second stage was operated under a constant voltage. Tanaka [27] presented a multi-stage ED computer model that combines multiple stacks in series. McGovern et al. [7, 28] used a counterflow ED system coupled with reverse osmosis to decrease the costs of water production.

Even though these ideas have been previously presented in the literature, there has not been a detailed study on how to make the best use of multi-stage ED, and on the effect of these configurations on the performance of ED systems. In particular, there has been no mention of how current densities (or voltages) in each stage should be chosen, or how two-stage ED compares to single-stage ED, and how counterflow ED compares to parallel-flow ED.

In this paper, we study possible improvements to the energy efficiency of electrodialysis through the use of two electric stages, and through the operation in counterflow configuration. We start by introducing some ideas from the literature that are necessary to explain the results that follow, such as the theorem of equipartition of entropy generation [18] and the concept of the equipartition factor [29]. We then look at how a two-stage ED system should be operated for optimal energy efficiency. In addition, we quantify the energetic benefits of two-staging in cost-effective brackish-water desalination and high-salinity brine concentration ED systems. Finally, we study the effect of operating in counterflow on these two applications.

2. Equipartition of entropy generation

In this section, we present some concepts that are necessary to interpret the results presented in this study. A good starting point is to present the motivation behind trying to reduce the rate of entropy generation. For a desalination system with fixed inlet and outlet flow rates and salinities, reducing the rate of entropy generation reduces the system's power consumption:

$$P = P_{\text{least}} + T_0 \dot{S}_{\text{gen}} \tag{1}$$

where the least power, P_{least}, is only a function of the inlet and outlet states and is fixed. T_0 is the temperature (of the environment and of the system), and $\dot{S}_{\text{gen}}$ is the rate of entropy generation. The derivation of the

equation above involves combining the First and Second Laws of thermodynamics, and can be found in a previous study [30].

As mentioned in Section 1, an important concept in the reduction of entropy generation is that of equipartition of entropy generation, first introduced by Tondeur and Kvaalen [18]. For a given system size operated continuously at steady state, and for a given total duty, the rate of entropy generation is minimized when its spatial variance is minimized. This theorem can be proven by using the Cauchy-Schwarz inequality when the phenomenological coefficient, L, which is the proportionality constant between the flux and the driving force, is assumed constant in the following relationship:

$$j = Lf \tag{2}$$

where j is the flux and f is the associated driving force, defined as

$$f \equiv \nabla \left(\frac{\partial S}{\partial X} \right) \tag{3}$$

where S is the entropy, and X is the quantity being transported (e.g., the number of moles of a species).

The local rate of entropy generation per unit volume is the product of the flux and the driving force:

$$\dot{s}'''_{\text{gen}} = jf = Lf^2 = \frac{j^2}{L} \tag{4}$$

When L is constant, the variance of the rate of entropy generation is minimized when the variance of the driving force and that of the flux are minimized.

The theorem is expressed by Tondeur and Kvaalen [18] by writing the following expression

$$\dot{S}_{\text{gen}} - \dot{S}_{\text{gen, equip}} = L\sigma^2 (f) > 0 \tag{5}$$

which shows that the rate of entropy generation is always larger than that of the equipartitioned system, where $\sigma (f)$ is the variance of the driving force.

Johannessen et al. [31] have shown that, even when L is not constant, the total rate of entropy generation is minimized when the variance of the entropy generation is minimized. In their study, minimizing the variance of the driving force led to a very similar total rate of entropy generation even though the temperature profiles in the heat exchanger were different. The explanation they provide for this result is that the variation of the entropy generation around its minimum is flat.

In addition, Johannessen and Kjelstrup [32] showed that the theorem of equipartition of entropy generation

also relies on the assumption that all the driving forces in the system can be controlled independently. However, Magnanelli et al. [33] showed that the equipartition of entropy generation yields a result that is very close to the numerical optimum even when this condition is not met, and can therefore be used in designing systems for improved operation.

As a result of the theorem of equipartition of entropy generation, the total rate of entropy generation can be divided into two parts. The first part is the rate that arises if the variance of rate of entropy generation is set to zero, and which Thiel et al. [29] refer to as the rate of entropy generation of the equivalent equipartitioned system, $\dot{S}_{\text{gen, equip}}$. The second part is the rate of entropy generation that arises due to the imbalance in the distribution of the rate of entropy generation, $\dot{S}_{\text{gen, imbalance}}$. We can write:

$$\dot{S}_{\text{gen, total}} = \dot{S}_{\text{gen, equip}} + \dot{S}_{\text{gen, imbalance}} \tag{6}$$

For a given transport area, A, and a given duty, J, which is transported over a distance h, $\dot{S}_{\text{gen, equip}}$ is constant. For a constant phenomenological coefficient, L, we can write:

$$\dot{S}_{\text{gen, equip}} = \int \dot{s}'''_{\text{gen}}\, dV = \bar{j}\bar{f}hA = \frac{J^2 h}{LA} \tag{7}$$

where $\bar{f}$ is the mean driving force, and $\bar{j}$ is the mean flux:

$$\bar{j} = L\bar{f} = \frac{J}{A} \tag{8}$$

As a result, for a fixed system size and a fixed phenomenological coefficient, changing the distribution of the flux through better use of operating degrees of freedom only affects the rate of entropy generation due to imbalance, $\dot{S}_{\text{gen, imbalance}}$.

The extent of the performance improvement that arises from better operation is captured by the equipartition factor, Ξ, as defined by Thiel et al. [29]:

$$\Xi \equiv \frac{\dot{S}_{\text{gen, equip}}}{\dot{S}_{\text{gen, total}}} \tag{9}$$

If a very large fraction of the total rate of entropy generation is simply due to a large mean flux, which is in turn due to a small system size, resulting in a high equipartition factor, no significant improvements to the system performance can be made by better distributing the rate of entropy generation. In other words, even if the system operation is changed to result in zero variance of the rate of entropy generation, the total rate of entropy generation does not change greatly, and the performance is barely affected. A low equipartition

factor means that a significant fraction of the total rate of entropy generation is due to a poor distribution of the flux, which means that significant improvements can be made without increasing the system size if the variance is decreased through better operation. We note that it is difficult to calculate the equipartition factor when the phenomenological coefficient is not constant without fully modeling the equipartitioned system.

2.1. Applying the theorem of equipartition of entropy generation to ED systems

We now apply the theorem of equipartition of entropy generation to ED. The local rate of entropy generation that arises from the transport of a single species is the product of the species flux and its driving force. For the transport of n species, the rate of entropy generation per unit area can be written as [30, 34, 35]:

$$\dot{s}''_{\text{gen}} = \sum_{i}^{n} j_i \Delta \left(\frac{-\mu_i}{T} \right) \tag{10}$$

where j_i is the flux of species i, μ is the electrochemical potential, and T is the absolute temperature. As explained in detail in Appendix B, some approximations can be made, and Eq. 10 can be simplified to result in the following expression:

$$\dot{s}''_{\text{gen}} = j_{\text{s}} \left(\frac{F V_{\text{cp}} - \Delta \mu_{\text{s}}}{T} \right) \tag{11}$$

where j_{s} is the salt flux, F is the Faraday constant, V_{cp} is the cell-pair voltage, and $\Delta \mu_{\text{s}}$ is the difference in the salt chemical potential between the concentrate and the diluate. In addition, it is helpful to think about the flux in terms of the current density, which is easier to measure in practical systems:

$$i \approx F j_s \tag{12}$$

where the current utilization rate is assumed to be very close to 1. We note that Eq. 11 and Eq. 12 are only used to give a clearer picture of how entropy generation can be related to current density and voltage, and that, in the calculated results presented in this paper, the full expression for entropy generation, Eq. 10, is used along with the full modeling approach detailed in Section 3.

For an electrodialysis system, the quantity transported (or the "duty") is the total rate of salt transport in mol/s. If the phenomenological coefficient linking the salt flux to the driving force is assumed constant, equipartition of entropy generation would state that the variances of the driving force and the flux need to be minimized. However, in ED L is not constant because the stack resistance can be a strong function of the concentrations, which are changing over the length of the system. When the assumption of a constant L breaks down, no single operating point can at once minimize the variances of the flux, the driving force, and the rate of entropy generation. The effect of a varying L on equipartition of entropy generation in ED

is investigated in Section 4.

3. Modeling

In this section, we summarize the components of the ED models used. In addition, we present the system configuration and constraints, and a brief overview of the solution method.

3.1. Local transport

At any location in an ED stack, given the cell-pair voltage and the diluate and concentrate concentrations, we can calculate the local species fluxes and the current density. To account for the effect of fluid flow on the mass transfer, the stagnant film model is used, which is common in system-level ED modeling [7, 8, 36–38]. It is too computationally intensive to model the full Navier-Stokes equations over an entire system length. The stagnant film model assumes that the fluid is very well mixed everywhere inside the fluid channel, except for a thin concentration boundary layer adjacent to each membrane. The stronger the mass transfer, the thinner the diffusion film. The thickness of the diffusion film is calculated using Eq. D.1, which is the Sherwood number correlation developed by Kuroda et al. [39].

The cell-pair voltage is the sum of the voltage drops that occur in the channel (bulk and film) and in the membranes (including the solution-membrane interface):

$$V_{\mathrm{cp}} = (r_{\mathrm{bulk,C}} + r_{\mathrm{bulk,D}})\, i + \Sigma_{j=1}^{4} \Delta\Phi_{\mathrm{film,j}} + \Delta\Phi_{\mathrm{CEM}} + \Delta\Phi_{\mathrm{AEM}} \tag{13}$$

where i is the current density, $\Delta\Phi_{\mathrm{CEM}}$ and $\Delta\Phi_{\mathrm{AEM}}$ are the membrane potential drops, including the Donnan potentials of the adjacent interfaces. Details on the calculation of the membrane potential drops are shown in Appendix E and Appendix F. The concentrate and diluate bulk resistances, $r_{\mathrm{bulk,C}}$ and $r_{\mathrm{bulk,D}}$, are calculated using conductivity data for sodium chloride [40–42]. The motivation behind modeling sodium chloride is explained in Appendix C. The film electric potential drops, $\Delta\Phi_{\mathrm{film,j}}$, and the film concentration profiles are calculated using the Maxwell-Stefan equations, as explained in Appendix D. It is assumed that a large number of cell pairs is used, as is done in practice. As a result, most of the voltage drop will occur inside the membranes and the fluid channels, and the voltage drops at the two electrodes can be neglected. In addition, the calculations performed in this paper are on a per-cell-pair basis. As was shown in a previous publication [17], the number of cell pairs (if large enough to make the electrode potential drop negligible) does not affect the energetic performance of the ED system if the membrane area and the product of the width and the number of cell pairs are kept constant.

In modeling brackish-water desalination, we use the Maxwell-Stefan-based model developed by Kraaijeveld et al. [38], presented in Appendix E. The membranes characterized by Kraaijeveld et al. [38] are not suitable for high-salinity applications, so the model developed by Fidaleo and Moresi [37] is used to model the brine-concentration application, as is detailed in Appendix F.

The ED models used in this paper are among the most thorough in the literature. These models do not assume ideal transport (transport number equal to 1), and they allow the membrane perm-selectivity to vary with the concentrations of the concentrate and diluate solutions. In addition, the modeling approach used in this paper has previously been validated [17, 30, 43] using experimental results from the literature [36, 44].

The local transport equations are integrated over the length of the system through the use of finite differences. This also allows the calculation of the variances of the different quantities needed in this analysis.

3.2. System constrains and configuration

To be able to compare the power consumption of the different operating points, the system size is held constant. As was done in a previous study [17], the fixed costs of the system are assumed to depend only on its size, represented by the total cell-pair membrane area. In addition, the feed flow rate and salinity, and the product flow rate and salinity are kept constant to allow a fair comparison between the different operating points.

When the area of a single-stage system is fixed, there is only one voltage that results in the set outlet salinities. In a two-stage system, the total available area is divided between two stages, each operated at a different voltage, as shown in Fig. 1. Because the total area is fixed, setting the fraction of area that goes into the first stage automatically sets the fraction that goes into the second, resulting in one degree of freedom. By choosing the voltage of the first stage, V_1, as the second degree of freedom, the voltage of the second stage, V_2, is set because the outlet salinities are fixed.

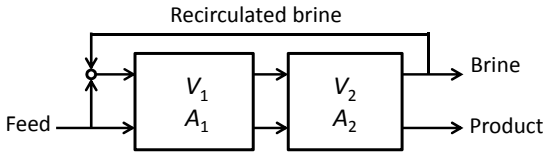

Fig. 1: Schematic diagram of a two-stage ED system with brine recirculation. A single-stage system will have $V_1 = V_2$, whereas a two-stage system will have different voltages. The fixed costs of the two systems, represented by their size, will be the same. The number of electrodes used in both configurations will also be the same.

The degree of brine recirculation is determined by the set recovery, defined as the ratio of the mass flow rate of the product stream (i.e., diluate stream in desalination and brine stream in salt production) over the mass flow rate of the feed. Given that the volumetric flow rates of the two streams are affected by water transport, only the outlet streams of the stack are fixed. For this reason, the system is solved starting at the

outlets, and using species balance to build the concentration and current density profiles to get to the inlets. At the inlets, species balance is performed to check that the calculated concentrations are correct.

In studying the effect of multi-staging and counterflow operation, it is not necessary to consider pumping power because it can be assumed constant. This is possible because the velocity, length of stack (in the direction of fluid flow), and channel height are held constant, and entry effects are negligible compared to the pressure loss in the stack [17]. The velocity is fixed to values determined in our previous cost minimization study [17].

4. The optimal operation of a two-stage ED system

Operating a system of fixed total area under two voltages results in two degrees of freedom: the fraction of the area that goes into the first stage, and the voltage of the first-stage. In this section, we look at how these two variables should be chosen to result in the best energetic performance.

4.1. Effect of the voltage of the first stage on power consumption

First, we study the effect of V_1 on the energy consumption of the system. This is done by dividing the total length equally between the two stages. In this section, a feed of brackish water at 3 g/kg is desalinated to result in a product at 0.35 g/kg at a recovery of 80%. The applications considered in this study are summarized in Table 1. To magnify the effect of two-staging, a large system is modeled: the stack length is 5 m, double the cost-effective value calculated for this application [17]. A channel height value of 0.5 mm and a velocity of 18 cm/s are also taken from our previous study [17].

Table 1: Summary of the conditions of the three applications studied.

Application	**Feed salinity [g/kg]**	**Product salinity [g/kg]**	**Recovery ratio [%]**
Brackish-water desalination	3	0.35	80
Partial seawater desalination	35	1	70
High-salinity brine concentration	70	200	21

As shown in Fig. 2(a), there exists a value of the first-stage voltage that minimizes the stack power consumption. As shown in Fig. 2(b), this is the same value that minimizes the total rate of entropy generation, as expected from Eq. 1. The first-stage voltage is normalized by the single-stage voltage:

$$V_1^* = \frac{V_1}{V_{\text{single}}} \tag{14}$$

Thus, a single-stage system is that corresponding to a normalized first-stage voltage of 1. For this case of

brackish water desalination, the reduction in power consumption is around 6% compared to the single-stage system.

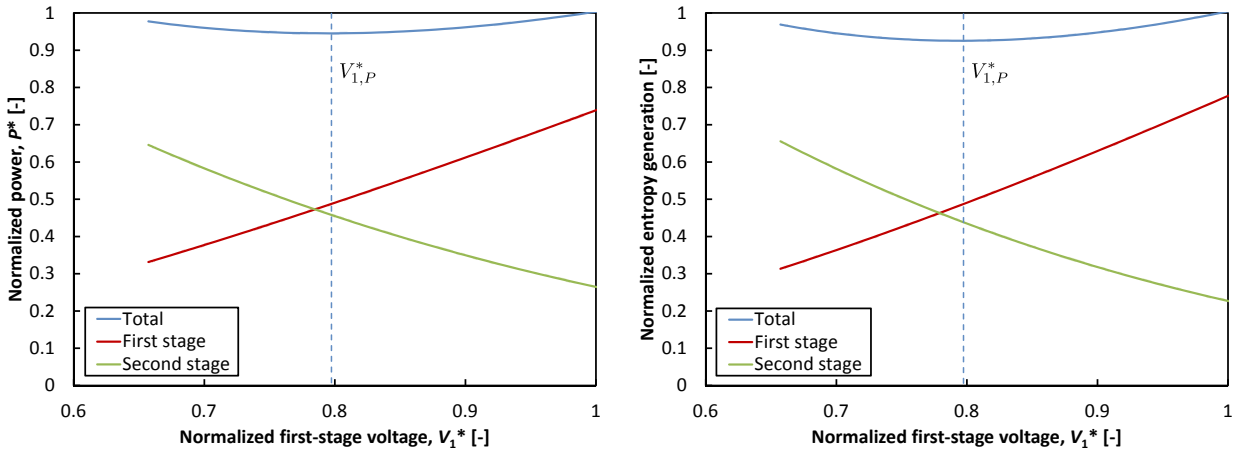

(a) The effect of the voltage of the first stage on the power consumption of a two-stage system.

(b) The effect of the voltage of the first stage on the entropy generation of a two-stage system.

Fig. 2: The effect of the voltage of the first stage on the power consumption of a two-stage system. The first-stage voltage, the power, and the entropy generation are normalized by their single-stage values. $S_{\text{feed}} = 3$ g/kg. See Table 1 for conditions.

As shown in Fig. 3, the voltage of the first stage affects the performance of the system by changing the distribution of the current density. As the first-stage voltage increases, more salt is transported in the first stage and less in the second. The voltage that yields the lowest power consumption, indicated by the vertical dashed line, yields a better distribution of current density between the first and the second stage than the single-stage system represented by a normalized first-stage voltage of 1. This also yields a better spatial distribution of the rate of entropy generation. In fact, as shown in Fig. 4, the voltage that minimizes power consumption and total entropy generation, $V^*_{1,P}$, is equal to that which minimizes the variance of the rate of entropy generation, $V^*_{1,\text{Var}(\dot{s}''_{\text{gen}})}$, and is higher than the first-stage voltage that minimizes the variance of the current density, $V^*_{1,\text{Var}(i)}$:

$$V^*_{1,P} = V^*_{1,\text{Var}(\dot{s}''_{\text{gen}})} > V^*_{1,\text{Var}(i)}$$

This result is consistent with the conclusion by Johannessen et al. [31] that, for a system with a varying phenomenological coefficient, the rate of entropy generation is what fundamentally needs to be equipartitioned, and not the flux or the driving force. In this case, minimization of the variance of the current density results in a power consumption that is 1.6% higher than the optimal. The variances of the three quantities are minimized at the same operating point only when the phenomenological coefficient is constant.

To better illustrate how the voltage of the first stage lowers the total rate of entropy generation, the current density and entropy generation profiles of the optimal two-stage system are compared to those of the single-stage system in Fig. 5. The single-stage system does not make good use of the membrane area towards

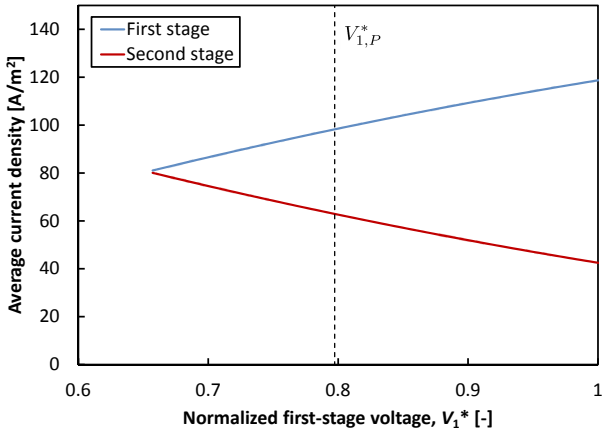

Fig. 3: The effect of the voltage of the first stage on the average current density in each stage. The first-stage voltage is normalized by the single-stage voltage. $S_{\text{feed}} = 3$ g/kg. See Table 1 for conditions.

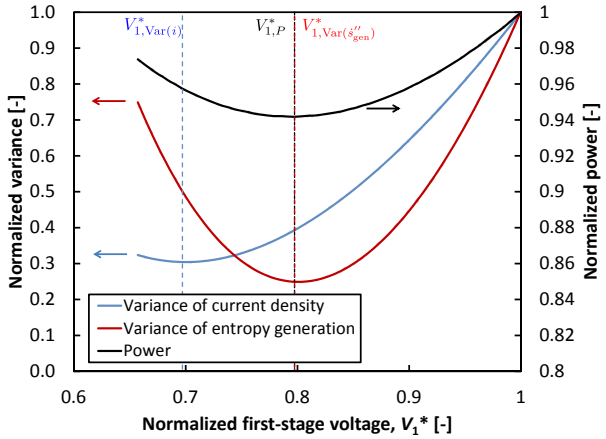

Fig. 4: The effect of the voltage of the first stage on the variance of the current density, the variance of the rate of entropy generation, and the power consumption for brackish-water desalination where osmosis and diffusion are negligible. The variables are normalized by their single-stage values. $S_{\text{feed}} = 3$ g/kg. See Table 1 for conditions.

the end of the stack because the current density is low. To compensate for the low current density at the end of the stack, the single-stage voltage has to be set to a high value, which results in a high current density at the inlet of the stack. The two-stage system overcomes this problem by having a low voltage in the first stage, and a higher voltage in the second stage, ensuring a better distribution of the current density and of the entropy generation rate, and a better usage of the available membrane area. This results in the reduction of the required power consumption.

4.2. Effect of osmosis and diffusion on the optimal operation of two-stage ED

In some ED applications, the concentration difference between the concentrate and diluate channels can be large, resulting in significant losses due to osmosis and diffusion. In such cases, when the inlet and outlet salinities and flow rates are fixed, different operating conditions can result in different rates of osmosis and diffusion. In the case of a two-stage system, a higher voltage in the first stage results in a faster increase

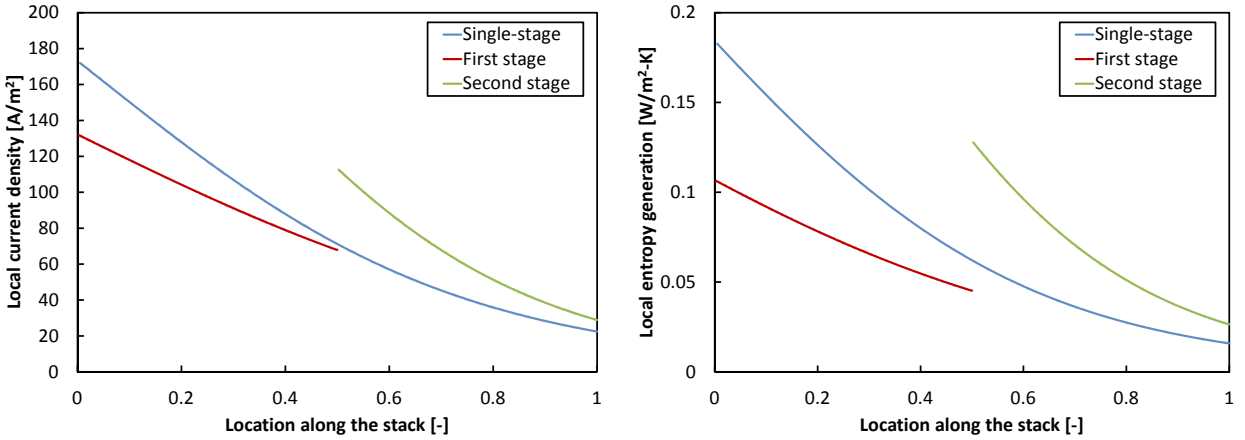

(a) The distribution of the current density along the streamwise direction.

(b) The distribution of the rate of entropy generation along the streamwise direction.

Fig. 5: The distribution of the current density and of the rate of entropy generation along the length of the stack for a single-stage system and for the optimal two-stage system. In this case, operating under two voltages results in a 5% reduction in power consumption compared to the single-stage system. $S_{\text{feed}} = 3$ g/kg. See Table 1 for conditions.

in the difference in concentration between the concentrate and the diluate channels. A higher concentration difference in the second stage over the same membrane area results in more osmosis and diffusion, which in turn result in a larger amount of salt that needs to be removed from the diluate to the concentrate, and a larger required current. The increasing average current density with increasing first-stage voltage is shown in Fig. 6 for the desalination of a feed from 35 g/kg to 1 g/kg at a recovery of 70% and a system length of 12 m. By contrast, the average current density in the case shown in Fig. 4 was constant for the full range of the first-stage voltage because the smaller concentration difference does not result in significant osmosis and diffusion.

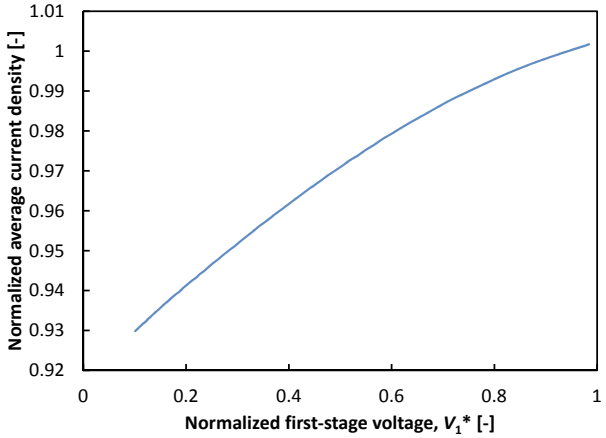

Fig. 6: The effect of the voltage of the first stage on the average current density of the system. The variables are normalized by their single-stage values. $S_{\text{feed}} = 35$ g/kg. See Table 1 for conditions.

The variation of the current with the first-stage voltage, which indicates a variation in the salt flux,

violates the condition of fixed duty that is required by the theorem of equipartition of entropy generation. As a result, as shown in Fig. 7, the voltage that minimizes power consumption and total entropy generation, $V^*_{1,P}$, is lower than the voltage that minimizes the variance of the rate of entropy generation, $V^*_{1,\mathrm{Var}(\dot{s}''_{\mathrm{gen}})}$:

$$V^*_{1,P} < V^*_{1,\mathrm{Var}(\dot{s}''_{\mathrm{gen}})}$$

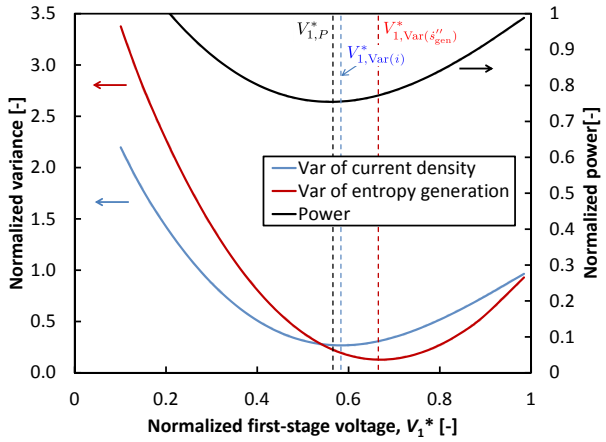

Fig. 7: The effect of the voltage of the first stage on the variance of the current density, the variance of the rate of entropy generation, and the power consumption. The variables are normalized by their single-stage values. $S_{\mathrm{feed}} = 35$ g/kg. See Table 1 for conditions.

As shown by Eq. 6, the total rate of entropy generation can be thought of as consisting of two parts. The first part of Eq. 6, which is proportional to the average of the flux, is minimized when the current is minimized, and this behavior favors a lower value of the first-stage voltage. The second part, due to the imbalance in the system, is minimized when the variance of the entropy generation is minimized. As a result of these two effects, the voltage that minimizes the total rate of entropy generation is lower than that which minimizes the variance of the rate of entropy generation when osmosis and diffusion are non-negligible. In the case studied in Fig. 7, the optimal first-stage voltage is closer to that which minimizes the variance of the current density.

In summary, in the absence of osmosis and diffusion, the voltage of the first stage should be set such that the variance of the rate of entropy generation is minimized. When osmosis and diffusion are non-negligible, the optimal first-stage voltage is smaller than that which minimizes the variance of the rate of entropy generation because a smaller first-stage voltage results in lower osmotic and diffusive losses, and in a lower duty. The optimal operating point is determined by the trade-off between the reduction in duty and the reduction in the variance of the rate of entropy generation.

4.3. Effect of the distribution of area between the two stages on power consumption

Next, we turn to the effect of the distribution of area between the two stages on the power consumption. We consider the desalination of a feed from 35 g/kg to 1 g/kg at a recovery of 70% and a system length of 12 m. At each division of area, the voltage of the first stage is set such that the power consumption is minimized. The distribution of the available area provides an additional degree of freedom which can be used to decrease the total rate of entropy generation for a fixed system size.

Figure 8 shows that the total power consumption is minimized when around 80% of the total area is used in the first stage, which is the distribution of area that also minimizes the variance of rate of entropy generation and the average current density. The power consumption is reduced by 29% compared to the single-stage system, and by 7% compared to the two-stage system with equal distribution of area between the two stages. As shown by the mostly flat variation of power consumption in Fig. 8, most of the gains of two-staging can be realized even if the distribution of area between the two stages is not optimal. The reduction in power consumption compared to the single-stage system is significant because the modeled desalination application is highly favorable to multi-staging due to its small equipartition factor, as defined in Eq. 9. The wide range of salinity covered by the system ensures a large change in resistance and current density over the length of the system, which, at a fixed voltage, results in a large variability in the rate of entropy generation. In addition, a large system size results in a lower rate of entropy generation that is due to the average flux (see Eq. 7), and magnifies the effect of multi-staging on the system energy consumption, as explained in Section 2.

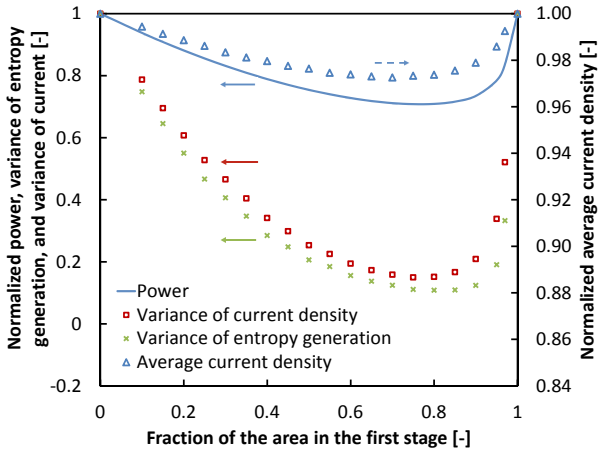

Fig. 8: The effect of the distribution of area between the two stages on the power consumption, the variance of the current density, the variance of the rate of entropy generation, and the average current density. The variables are normalized by their single-stage values. $S_{\text{feed}} = 35$ g/kg. See Table 1 for conditions.

In addition, the choice of the first-stage length (while keeping the system length constant) can serve to decrease the average current density. The average current density is decreased by around 3% for a first-stage fraction of around 70%. This is an indication that the choice of the distribution of area can decrease osmosis

and diffusion by making the available area smaller when the salinity difference between the two streams is large, which is close to the outlet of the system. Even with the same inlet and outlet salinities for the system as a whole, the operation of the system dictates the distribution of the available area between the different parts of the process.

The optimal first-stage fraction of around 80% is specific to the system modeled in this section. Different inlet and outlet salinities have yielded first-stage fractions between 50% and 80%, with the applications with a higher salinity range yielding a larger first stage.

5. The benefits of multi-staging in brackish-water desalination and in high-salinity brine concentration

In the previous section, large systems were modeled to magnify the effects of two-staging in order to be able to study how a two-stage system should be operated. In this section, we quantify the benefits of multi-staging for system sizes that are cost-effective, and for ED applications that are already in use. We expect the benefits of multi-staging to increase with increasing system size, so it is important to choose cost-effective system sizes, which are smaller than those modeled in the previous section.

We study the effect of multi-staging on two applications: a) the desalination of a brackish-water feed from 3 g/kg to 0.35 g/kg at a recovery of 80%, and b) the concentration of highly-saline brine from 70 g/kg to 200 g/kg at a recovery of 21%. The first application is for the production of drinking water from brackish water, where the brine stream is recirculated to ensure high recovery. The second application is part of a salt production process, which uses as feed the brine outlet of a typical seawater desalination system. The recovery is set such that the diluate stream leaves the system at 35 g/kg, which is considered to match the salinity of seawater for convenience of discharge. The configuration used in the first application is the same as in Fig. 1. The configuration of the second application does not employ brine recirculation, and instead the flow rates of the diluate and concentrate channels have different values so as to produce the required recovery.

In a previous study [17], a cost model was used to determine the system size at which total costs are minimized for a single-stage system. In this section, we study the effect of operating under two voltages at the previously determined cost-effective system sizes and operating conditions such as the velocity. For each system size, the voltage of the first stage and the division of area between the first and second stages are set such that the power consumption is minimized.

5.1. The effect of multi-staging on brackish-water desalination

At a cost ratio of 134 W/m^2 (see Appendix G) and for a channel height of 0.5 mm, the optimal effective length for this application is 2.5 m and the optimal fluid velocity, determined by a trade-off between ED electric power and pumping power, is 18 cm/s [17]. As shown in Fig. 9, at the cost-optimal length of 2.5 m, operating under two voltages only reduces the power consumption by less than 1%, and the improvement in the energetic performance reaches less than 6% at a length of 5 m, which is double the cost-optimal length. The effect of multi-staging is not large because fixed costs are very high; and, as shown in a previous study [17], the ED system is operated close to the limiting current density, which means that the system size that minimizes the total costs is fairly small. A small system size results in a large rate of entropy generation that is due to the average flux, which reduces the importance of the rate of entropy generation that is due to the variance of the flux. In other words, the cost-optimal ED system for brackish-water desalination has a high equipartition factor, and, even if the variance in the rate of entropy generation is minimized, the total rate of entropy generation does not vary greatly.

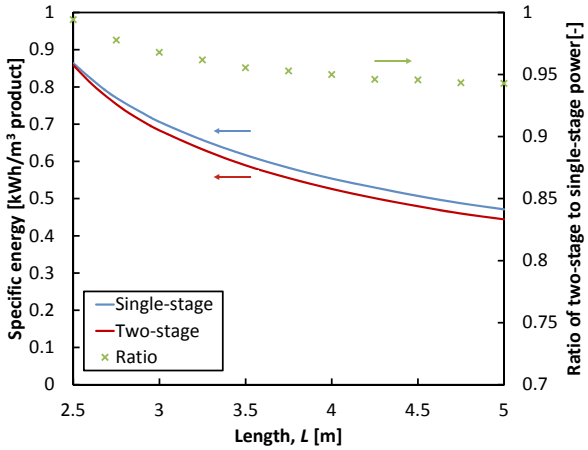

Fig. 9: The effect of the length of the system on the power consumption of single-stage and two-stage systems for brackish-water desalination. The cost-optimal length for the single-stage system is 2.5 m.

The results presented in Fig. 9 are for a cost ratio, r, equal to 134 W/m^2. If the cost ratio is reduced fivefold (to $r = 26$ W/m^2), operating under two voltages at the cost-optimal system size reduces the power consumption by slightly less than 5%. For two-stage operation to yield a significant reduction in power consumption and costs, the fixed costs of ED need to be much smaller relative to electricity costs than are those reported in Table G.5.

5.2. The effect of multi-staging on high-salinity brine concentration

The effect of multi-staging is even lower in the brine concentration application. As shown in Fig. 10, operating under two voltages barely reduces the power consumption. In fact, the improvement is less than

2% for a length of 10 m, which is around 50% larger than the cost-optimal length of 6.6 m.

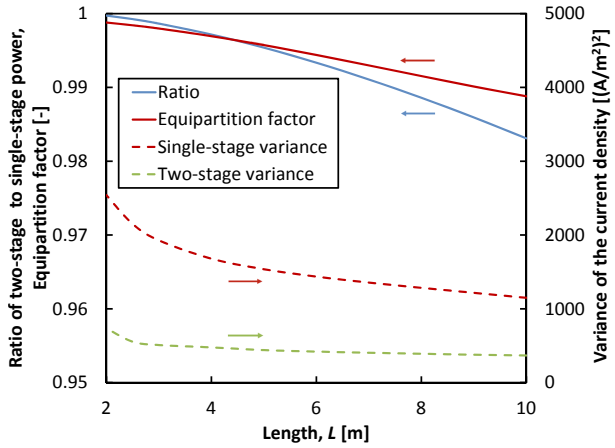

Fig. 10: The effect of the length of the system on the equipartition factor, the ratio of two-stage to single-stage power consumption, and on the variance of single-stage and two-stage systems for high-salinity brine concentration. The cost-optimal length for the single-stage system is 6.6 m.

The stack resistance at high salinity is dominated by the membrane resistance [30], which does not vary greatly with salinity. We can therefore approximate the equipartition factor by assuming a constant resistance, and Eq. 9 can be written as a function of the current density:

$$\Xi \approx \frac{\bar{i}^2}{\overline{i^2}} \tag{15}$$

where the numerator is the square of the average current density, and the denominator is the average of the square of the current density. As explained in Section 5.1, the high capital costs relative to energy costs push the optimum towards smaller systems and higher energy consumption, which explains why the equipartition factor for this application in the range of the cost-optimal system size is very high, as shown in Fig. 10.

Even though operating under two voltages significantly decreases the variance of the current density, as shown in Fig. 10, this decrease in variance barely affects the total rate of entropy generation, which is mostly due to the average of the flux, and not its variance, as shown by the high equipartition factor.

At first, a ratio of two-stage to single-stage power consumption that is lower than the equipartition factor seems contradictory. The equipartition factor sets the limit on the amount by which the total rate of entropy generation can be decreased if the entropy generation due to the imbalance, $\dot{S}_{\text{gen, imbalance}}$, is set to zero. However, it is also assumed that the entropy generation due to the mean will not change. In this case, the amount of salt that needs to be removed decreases slightly due to the decrease in osmosis and diffusion, which means that even the rate of entropy generation due to the mean decreases, which explains why the improvement in performance is slightly larger than the maximum predicted by the equipartition factor.

The effect of multi-staging in the high-salinity case is lower than that in the brackish-water case. This

can be explained by a higher equipartition factor in the brine-concentration application. At high salinity, the dominant resistance is that of the membranes, which does not vary greatly with salinity. This means that the variation of the concentrations along the stack affects the total resistance much less than in brackish-water applications, resulting in a lower variance of the rate of entropy generation. In addition, the entropy generation is much higher in the brine-concentration application because a lot more salt is being removed to take a feed from 70 g/kg to 200 g/kg than in taking a feed from 3 g/kg to 0.35 g/kg, resulting in a higher $\dot{S}_{\text{gen, equip}}$.

Finally, even if the cost ratio is reduced from 134 W/m^2 to around 40 W/m^2, the two-stage system at the cost-optimal size only reduces the power consumption by 2% relative to the single-stage system. In summary, current electrodialysis fixed costs need to be greatly reduced relative to the cost of electricity for two-staging to have significant effects on the power consumption of ED.

The effect of multi-staging on the energetic performance of cost-effective ED systems is summarized in Table 2.

Table 2: Summary of the effect of two-staging on the energetic performance of cost-effective ED systems for brackish-water desalination and high-salinity brine concentration.

Application	**Cost ratio [W/m^2]**	**Reduction of power consumption due to two-staging**
Brackish-water desalination	134	<1%
	26	5%
High-salinity brine concentration	134	<1%
	40	2%

6. Counterflow electrodialysis

In this section, we study the effect of operating in counterflow on the performance of ED systems. Operating in counterflow is expected to improve the distribution of the concentration difference. In a parallel flow ED system, the concentrations are close (or equal) at the inlet, and diverge as salt is transported from the diluate to the concentrate channel. In a counterflow system, the concentrations of the two streams are high on one end, and low at the other.

6.1. Brackish-water desalination

First, we look at the effect of operating in counterflow on the performance of a brackish-water desalination system. We compare a counterflow system to a parallel-flow system with the same inlets and outlets and

with the same system dimensions. By setting these constraints we can compare the energy consumption of the two systems fairly. In addition, we neglect any trans-membrane pressure drop that might arise from the operation in counterflow mode, which means that we are calculating a performance limit of the counterflow system, with practical systems yielding a lower performance due to leakage.

Figure 11 shows that operating in counterflow reduces the power consumption relative to the parallel-flow system by around 3-4%. We note that this improvement can be divided between a decrease in the required voltage, and a decrease in the total current, which represents the total amount of salt removed, and which quantifies the effects of osmosis and diffusion. In the brackish-water desalination application, the voltage is decreased by around 3% compared to the parallel-flow operation, which is due to a better distribution of the chemical potential difference, whereas the current is only decreased by less than 1%, which means that operating in counterflow does not greatly reduce osmosis and diffusion in this application. Operating in counterflow reduces the voltage that is required to overcome the concentration difference, and results in a better distribution of the rate of entropy generation, thus reducing the required power consumption by directly affecting the required voltage.

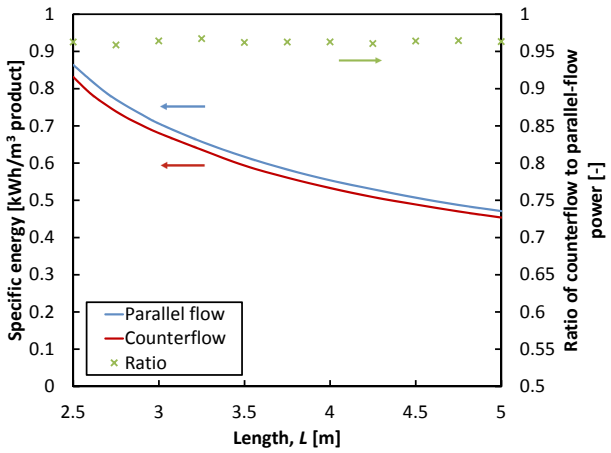

Fig. 11: The effect of the length of the system on the power consumption of parallel flow and counterflow ED systems for brackish-water desalination.

If the system length is increased to 15 m, a very significant size, a 6% reduction in power consumption can be achieved relative to the parallel-flow configuration. This shows that the effect of operation in counterflow increases with increasing system size. This is due to having a lower equipartition factor when the system size is increased.

For operation of counterflow to be preferred over operation in parallel flow, this improvement in performance would need to be greater than the negative effects that arise from operating in counterflow, including leakage through the membrane due to the resulting trans-membrane pressure difference, the additional strain on the membranes, and the increased piping complexity.

6.2. High-salinity brine concentration

The effect of operating in counterflow is even lower in the brine-concentration application. As shown in Fig. 12, operating in counterflow reduces the variance in the current density by up to 98%, but only reduces the power consumption by 2.5% at a length of 10 m. This again is a result of the very high equipartition factor, which is due to operating at high current density (small system size) and low variability in the resistance along the stack. In addition, even for the brine concentration application, operating in counterflow reduces the total current by less than 1%, which means that it does not have a great effect on diffusion and osmosis.

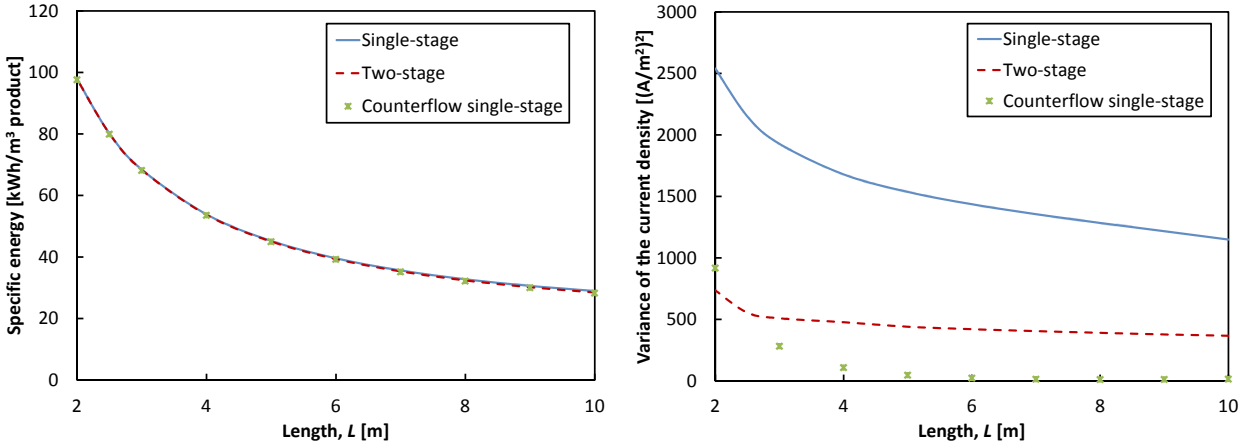

(a) The effect of system length on the power consumption.

(b) The effect of system length on the variance of the current density.

Fig. 12: The variation of the power consumption and variance of the current density with system length for a single-stage system, a two-stage system, and a counterflow single-stage system.

6.3. Differences between ED systems and heat exchangers

An ED stack, which can be thought of as a mass exchanger, has some significant differences from a heat exchanger. In a heat exchanger, we can think of the heat flux as being proportional to a temperature difference. By operating in counterflow, we make the streamwise distribution of the temperature difference more uniform, such that the temperature difference in no location along the exchanger is too small, as would happen in parallel flow, as shown in Fig. 13. By contrast, the driving force in an ED system is the difference in the electrochemical potential of the salt between the two streams, as shown in Eq. 11. Given that these systems are small and operate at high current densities, the contribution of the chemical potential difference to the electrochemical potential difference is small, as shown in Fig. 13. As a result, the variance of the chemical potential difference is small compared to the mean electrochemical potential difference, and a better distribution of the concentration difference does not have a great effect on performance. If ED fixed costs are reduced relative to energy costs, larger systems can be used and counterflow ED will have a bigger effect on the performance because the chemical potential difference forms a larger fraction of the applied voltage.

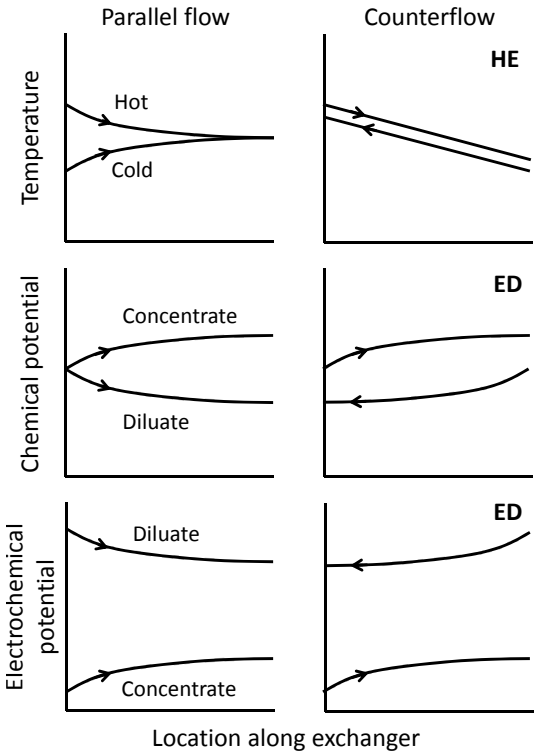

Fig. 13: Qualitative temperature profile in a heat exchanger, and chemical potential, and electrochemical potential profiles in an ED stack in parallel flow and in counterflow.

7. Conclusions

In this paper, we studied the effect of multi-staging ED and of operating ED in counterflow for brackish-water desalination and high-salinity brine concentration. We have shown that, in the absence of process-dependent losses such as osmosis and diffusion, the voltages in a multi-stage system should be set such that the spatial variance of the entropy generation rate is minimized, as predicted by the theorem of equipartition of entropy generation. When osmotic and diffusive losses are non-negligible, the total amount of salt that needs to be transported depends on the process, and equipartition of entropy generation is not enough to determine the optimal operating point because the condition of fixed duty does not hold. In such cases, the optimal first-stage voltage is determined by the trade-off between the reduction in duty and the reduction in the variance of the rate of entropy generation. In addition, the distribution of area between the two stages is another variable that can be used to decrease the power consumption by further decreasing the duty and the variance of the entropy generation rate.

Cost-effective ED systems tend to be small and are operated at high current density because of their high fixed costs relative to the cost of electricity. This results in a large rate of entropy generation that is due to the mean flux, which corresponds to a high equipartition factor. For system sizes that are cost effective, operating under two voltages does not have a big effect on the power consumption in brackish-

water desalination and in high-salinity brine concentration because the entropy generation that can be saved through the minimization of its spatial variance is a small fraction of the total rate of entropy generation. For these same reasons, operating in counterflow does not result in a significant decrease in power consumption compared to operating in parallel flow. When one considers the negative effects of operating in counterflow, the prospects become even less promising, if not negative.

If a large membrane area is used, and the stack resistance varies greatly over the length, the amount of entropy generation that is due to imbalance, $\dot{S}_{\text{gen, imbalance}}$, can be significant. It was shown that, in such cases, operating in two-stages can result in a significant reduction in a system's energy consumption (up to 29%). Future work on improving the energy efficiency of ED systems should therefore focus on reducing $\dot{S}_{\text{gen, equip}}$ as defined in Eq. 7, which can be done by decreasing the stack resistance or by decreasing ED fixed costs to allow the use of larger systems. This would allow the improved operation of ED to result in significant benefits.

Acknowledgments

The authors would like to thank the Kuwait Foundation for the Advancement of Sciences (KFAS) for their financial support through Project No. P31475EC01.

Appendix A. Limits on the benefits of system size increase

Increasing ED's system size decreases the power consumption only up to a certain critical size. The increase in area decreases the average salt flux, which reduces the rate of entropy generation, as shown in Eq. 7. However, in ED, there are losses in the form of osmosis and diffusion that also increase with the system size. At the critical system size, the marginal increase in area increases the losses due to osmosis and diffusion more than it decreases the losses due to the sought-after salt flux.

Appendix B. Driving force in electrodialysis

The local rate of entropy generation per unit area is the sum of the entropy generated by all the species:

$$\dot{s}''_{\text{gen}} = \sum_{i}^{n} j_i \, \Delta\left(\frac{-\mu_i}{T}\right) \tag{10}$$

where j_i is the flux of species i, T is the temperature, and μ_i is the electrochemical potential of species i:

$$\mu_i = RT \ln a_i + z_i F \Phi \tag{B.1}$$

where a_i is the activity of species i, and Φ is electric potential. For a binary salt, the species present are the cation, the anion, and the water. To obtain a simple expression, we assume perfectly perm-selective membranes, and we ignore water transport. The cation flux goes from the center of the diluate channel to the center of concentrate channel C_1 and the anion flux goes from the diluate channel to the concentrate channel C_2, as shown in Fig. B.14.

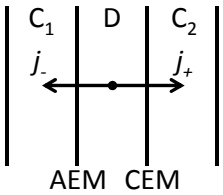

Fig. B.14: Schematic diagram showing the ion fluxes between the channels.

The two concentrate channels are at the same concentration, but at different electric potentials. We can write:

$$\dot{s}''_{\text{gen}} = j_{+,\text{CEM}} \left[RT \ln \frac{a_{+,\text{D}}}{a_{+,\text{C}}} + F \left(\Phi_{\text{D}} - \Phi_{\text{C}_2} \right) \right] \frac{1}{T} + j_{-,\text{AEM}} \left[RT \ln \frac{a_{-,\text{D}}}{a_{-,\text{C}}} - F \left(\Phi_{\text{D}} - \Phi_{\text{C}_1} \right) \right] \frac{1}{T} \tag{B.2}$$

For perfectly perm-selective membranes:

$$j_{\text{s}} = j_{+,\text{CEM}} = j_{-,\text{AEM}} \tag{B.3}$$

and

$$\dot{s}''_{\text{gen}} = j_{\text{s}} \left[F \left(\Phi_{\text{C}_1} - \Phi_{\text{C}_2} \right) - \left(\mu_{\text{s,C}} - \mu_{\text{s,D}} \right) \right] \frac{1}{T} = j_{\text{s}} \left(\frac{F V_{\text{cp}} - \Delta \mu_{\text{s}}}{T} \right) \tag{11}$$

where μ_{s} is the chemical potential of the salt. Even though the salt is neutral, the use of ion-exchange membranes results in the salt being driven by the electrochemical potential difference. This is clear from how ED uses an applied voltage to move salt from the diluate to the concentrate channel.

We note that Eq. 11 and the assumptions presented in this section are only used to give a clearer picture of how entropy generation can be related to current density and voltage, and that, in the calculated results presented in this paper, the full expression for entropy generation, Eq. 10, is used along with the full modeling approach detailed in Section 3.

Appendix C. Thermophysical properties

A solution of sodium chloride is modeled because of the availability of membrane data for both models used [36, 38]. In addition, the properties of sodium chloride can be used to approximate those of seawater [45,

46]. We use the implementation in MATLAB by Thiel et al. [47, 48] of Pitzer's equations [49–54]. The properties used are the solution density, the activity coefficient, the water activity, the osmotic pressure, and the ionic diffusivities.

Appendix D. Inside the diffusion films

The diffusion layer thickness, δ, is calculated from the correlation of the Sherwood number, Sh, by Kuroda et al. [39]:

$$\mathrm{Sh} = \frac{k_\mathrm{m} D_\mathrm{e}}{D} = \frac{D_\mathrm{e}}{\delta} = 0.25\ \mathrm{Re}^{\frac{1}{2}} \mathrm{Sc}^{\frac{1}{3}} \tag{D.1}$$

where k_m is the mass transfer coefficient, D is the diffusivity, Re is the Reynolds number, Sc is the Schmidt number. D_e is the effective diameter:

$$D_\mathrm{e} = \frac{2hW\left(1-\epsilon_\mathrm{s}\right)}{h+W} \tag{D.2}$$

W is the stack width, and is much larger than the channel height, h, so we can write:

$$D_\mathrm{e} = 2h\left(1-\epsilon_\mathrm{s}\right) \tag{D.3}$$

ϵ_s is the volume fraction in the channel, as reported by Kuroda et al. [39]. The Reynolds number and the Schmidt number are defined as:

$$\mathrm{Re} = \frac{\rho v D_\mathrm{e}}{\mu\left(1-\epsilon_\mathrm{s}\right)} = \frac{2\rho v h}{\mu} \tag{D.4}$$

$$\mathrm{Sc} = \frac{\mu}{\rho D} \tag{D.5}$$

where μ is the dynamic viscosity and ρ is the density.

In addition, electroneutrality is satisfied everywhere inside the diffusion film given that the interface is lumped with the membrane:

$$\sum_i z_i c_i = 0 \tag{D.6}$$

The film electric potential drops and the film concentration profiles are calculated by integrating the Maxwell-Stefan equations over the diffusion film using the fourth order Runge-Kutta method:

$$-\frac{c_i}{RT}\nabla\mu_i = \sum_{j=1}^{n} \frac{c_j j_i - c_i j_j}{c_\mathrm{tot}\, Đ_{ij}} \tag{D.7}$$

where c_i is the concentration of species i, μ_i is the electrochemical potential of species i, $Đ_{ij}$ is the Maxwell-Stefan diffusion coefficient of species i and j, and j_i is the molar flux of species i. The fluxes in the film are the same as those in the membranes due to conservation of species at steady state. The diffusion coefficients

inside the solution are adapted from Kraaijeveld et al. [38], with the original data from Chapman [55] and Mills and Lobo [56]:

$$Đ_{\mathrm{Na^+,H_2O}} = 1.333 \times 10^{-9}\ \mathrm{m^2/s} \tag{D.8}$$

$$Đ_{\mathrm{Cl^-,H_2O}} = 2.033 \times 10^{-9}\ \mathrm{m^2/s} \tag{D.9}$$

$$Đ_{\mathrm{Na^+,Cl^-}} = 0.0015c^{0.65} \times 10^{-9}\ \mathrm{m^2/s} \tag{D.10}$$

where c is the solution concentration in $\mathrm{mol/m^3}$.

Appendix E. Modeling transport through the membranes in brackish-water desalination

In modeling brackish-water desalination and seawater desalination, we use the Maxwell-Stefan-based model developed by Kraaijeveld et al. [38]. At each membrane-solution interface, each species that exists in both media is assumed to be in thermodynamic equilibrium:

$$\mu_i^{\mathrm{m}} = \mu_i^{\mathrm{s}} \tag{E.1}$$

Rearrangement of this equation allows the calculation of the Donnan potential drop at the interface:

$$\Delta\phi_{\mathrm{Donnan}} = \phi^m - \phi^s = \frac{RT}{z_i F} \ln \frac{a_i^s}{a_i^m} \tag{E.2}$$

Rearrangement of Eq. E.2 allows the calculation of the concentrations of the co-ion and counter-ion inside the membrane (in combination with electroneutrality inside the membrane):

$$\frac{c_+^s c_-^s}{c_+^m c_-^m} = \frac{\gamma_\pm^{m\,2}}{\gamma_\pm^{s\,2}} \tag{E.3}$$

where the activity coefficient of the salt inside the membrane, $\gamma_\pm^m$, was adapted from Kraaijeveld et al. [38], who fitted the coefficients using experimental data.

In addition, the Maxwell-Stefan equations are used to relate the fluxes through each membrane to the driving forces across the membrane. The diffusion coefficients inside the membrane are different from those in the channel and were measured by Kraaijeveld et al. [38, 44]. These equations are also used to calculate the electric potential drops across the membranes, which are added to the Donnan potential drops to form $\Delta\Phi_{\mathrm{m}}$ in Eq. 13. Details of this model have been presented in previous studies [17, 30, 38, 44], and our numerical implementation of this model has been validated in a previous work [30].

Table E.3: The diffusion coefficients inside the membranes (in 10^{-10} m^2/s) adapted from Kraaijeveld et al. [38].

Components	**61 CZL 386**	**204 UZL 386**
Na^+, Cl^-	0.24	0.19
Na^+, H_2O	3.12	0.75
Na^+, Membrane	0.31	0.16
Cl^-, H_2O	1.81	5.12
Cl^-, Membrane	0.31	0.51
H_2O, Membrane	2.49	4.93

Table E.4: Membrane characteristics measured by Kraaijeveld et al. [38]. c is the solution concentration in mol/L.

Membrane property	**61 CZL 386**	**204 UZL 386**
Capacity [mol/m^3 wet membrane]	1690	1827
Thickness [mm]	0.563	0.551
Density of wet membrane, ρ_m [kg/m^3]	1167.5 - $7.5c$ + $7.5c^2$	1100.0 + $15.0c$
Salt activity coefficient, $\gamma_{\pm}^{m}$ [-]	0.57 + $0.28c$	0.56 + $0.29c$
Water content [%]	30.17 - $0.83c$	33.38 - $1.42c$

The water concentration inside the membrane is calculated as follows:

$$c_w^m = \frac{\%H_2O \times \rho_m}{100 M_w} \tag{E.4}$$

where $\%H_2O$ is the water content inside the membrane.

Appendix F. Modeling transport through the membranes in high-salinity brine concentration

The model developed by Fidaleo and Moresi [37] is used to model the brine-concentration application. This model expresses the salt flux as the sum of contributions from current passage and back-diffusion:

$$j_s = \frac{T_s i}{F} - L_s \left(c_{s,C,m} - c_{s,D,m} \right) \tag{F.1}$$

and the water flux as the sum of contributions from electro-osmosis and osmosis:

$$j_w = \frac{T_w i}{F} + L_w \left(\pi_{C,m} - \pi_{D,m} \right) \tag{F.2}$$

where $c_{\mathrm{s,D,m}}$ is the salt concentration at the membrane interface in the diluate channel, $\pi_{\mathrm{C,m}}$ is the osmotic pressure at the membrane interface in the concentrate channel. T_{s} and T_{w} are the salt and water transport numbers, respectively, and L_{s} and L_{w} are the salt and water permeabilities respectively. These parameters were measured by McGovern at al. [36] for the Neosepta AMX-SB and CMX-SB membranes at salinities of up to 200 g/kg and are summarized below:

$$T_{\mathrm{s}} = -4 \times 10^{-6} S_{\mathrm{D}}^2 + 4 \times 10^{-5} S_{\mathrm{D}} + 0.96 \tag{F.3}$$

$$T_{\mathrm{w}} = -4 \times 10^{-5} S_{\mathrm{C}}^2 - 1.9 \times 10^{-5} S_{\mathrm{C}} + 11.2 \tag{F.4}$$

$$L_{\mathrm{s}} = 2 \times 10^{-12} S_{\mathrm{D}}^2 - 3 \times 10^{-10} S_{\mathrm{D}} + 6 \times 10^{-8} [\mathrm{m/s}] \tag{F.5}$$

$$L_{\mathrm{w}} = 5 \times 10^{-4} S_{\mathrm{C}}^{-0.416} [\mathrm{mol/m^2\text{-}s\text{-}bar}] \tag{F.6}$$

The membrane electric potential drop in Eq. 13 is

$$\Delta\Phi_{\mathrm{CEM}} + \Delta\Phi_{\mathrm{AEM}} = 2 r_{\mathrm{m}} i + \frac{\Delta\mu_{\mathrm{s}}}{F} = 2 r_{\mathrm{m}} i + 2 \frac{RT}{F} \ln \frac{\gamma_{\pm,\mathrm{C}} m_{\mathrm{C,m}}}{\gamma_{\pm,\mathrm{D}} m_{\mathrm{D,m}}} \tag{F.7}$$

where $\gamma_{\pm}$ is the mean molal activity coefficient, and m is the molality. The resistances of the membranes, r_{m}, was measured by McGovern et al. [36]:

$$r_{\mathrm{m}} = r_{\mathrm{CEM}} = r_{\mathrm{AEM}} = 3.5 \times 10^{-4}\ \Omega\ \mathrm{m}^2 \tag{F.8}$$

Our implementation of this model has been validated with experimental results from McGovern et al. [36] in a previous study [17].

Appendix G. Cost modeling

The cost-optimal system size is a strong function of the relative importance of fixed and operating costs. The cost ratio, r, was used by Chehayeb et al. [17] to capture this variability, where the normalized cost was defined as:

$$c^* = \frac{C}{K_{\mathrm{e}}} = rA + P \tag{G.1}$$

where A is the effective cell-pair area, P is the power consumption, and the cost ratio is defined as:

$$r = \frac{K_{\mathrm{m}}}{K_{\mathrm{e}}} \tag{G.2}$$

where K_e is the cost of electricity and K_m is the fixed cost per unit effective cell-pair area per unit time:

$$K_\mathrm{m} = \frac{K_{\mathrm{m},0}}{\frac{1}{i}\left[1 - \left(\frac{1}{1+i}\right)^{\tau}\right]} \tag{G.3}$$

where $K_{\mathrm{m},0}$ is the present value of the equipment costs. The values used in the calculation of the cost ratio are given in Table G.5.

Table G.5: The variables used in the cost modeling [36]. The resulting cost ratio is $r = 134$ W/m^2.

Variable	**Value**
Cost of electricity, K_e	\$0.15/kWh
Present value of equipment costs, $K_{\mathrm{m},0}$	$\$1,500/\mathrm{m}^2$ effective cell pair
Rate of return on capital, i	10%
Plant life, τ	20 years

References

[1] H. J. Lee, F. Sarfert, H. Strathmann, S. H. Moon, Designing of an electrodialysis desalination plant, Desalination 142 (2002) 267–286. doi:10.1016/S0011-9164(02)00208-4.
URL http://dx.doi.org/10.1016/S0011-9164(02)00208-4

[2] J. Ortiz, E. Expósito, F. Gallud, V. García-García, V. Montiel, A. Aldaz, Desalination of underground brackish waters using an electrodialysis system powered directly by photovoltaic energy, Solar Energy Materials and Solar Cells 92 (12) (2008) 1677–1688. doi:10.1016/j.solmat.2008.07.020.
URL http://linkinghub.elsevier.com/retrieve/pii/S0927024808002535

[3] H. Strathmann, Electrodialysis, a mature technology with a multitude of new applications, Desalination 264 (2010) 268–288. doi:10.1016/j.desal.2010.04.069.
URL http://dx.doi.org/10.1016/j.desal.2010.04.069

[4] N. C. Wright, A. G. Winter V, Justification for community-scale photovoltaic-powered electrodialysis desalination systems for inland rural villages in India, Desalination 352 (2014) 82–91. doi:10.1016/j.desal.2014.07.035.
URL http://dx.doi.org/10.1016/j.desal.2014.07.035

[5] W. E. Katz, The electrodialysis reversal (EDR) process, Desalination 28 (1) (1979) 31–40. doi:10.1016/S0011-9164(00)88124-2.

[6] A. E. R. Reahl, Half A Century of Desalination With Electrodialysis, Tech. rep., General Electric Company (2006).

[7] R. K. McGovern, S. M. Zubair, J. H. Lienhard V, The benefits of hybridising electrodialysis with reverse osmosis, Journal of Membrane Science 469 (2014) 326–335. doi:10.1016/j.memsci.2014.06.040.
URL http://dx.doi.org/10.1016/j.memsci.2014.06.040

[8] R. K. McGovern, S. M. Zubair, J. H. Lienhard V, The cost effectiveness of electrodialysis for diverse salinity applications, Desalination 348 (2014) 57–65. doi:10.1016/j.desal.2014.06.010.
URL http://dx.doi.org/10.1016/j.desal.2014.06.010

[9] M. Turek, Cost effective electrodialytic seawater desalination, Desalination 153 (2003) 371–376. doi:10.1016/S0011-9164(02)01130-X.

[10] M. Turek, Dual-purpose desalination-salt production electrodialysis, Desalination 153 (2003) 377–381. doi:10.1016/S0011-9164(02)01131-1.

[11] T. Mohammadi, A. Kaviani, Water shortage and seawater desalination by electrodialysis, Desalination 158 (2003) 267–270. doi:10.1016/S0011-9164(03)00462-4.

[12] M. Sadrzadeh, T. Mohammadi, Sea water desalination using electrodialysis, Desalination 221 (2008) 440–447. doi:10.1016/j.desal.2007.01.103.

[13] Y. Kobuchi, Y. Terada, Y. Tani, The First Salt Plant in the Middle East Using Electrodialysis and Ion Exchange Membranes, Sixth International Symposium on Salt ll (1983) 541–555.

[14] T. Nishiwaki, Concentration of electrolytes prior to evaporation with an electromembrane process, in: R. E. Lacey, S. Loeb (Eds.), Industrial Processing with Membranes, Wiley & Sons, 1972.

[15] Y. Zhang, K. Ghyselbrecht, B. Meesschaert, L. Pinoy, B. Van der Bruggen, Electrodialysis on RO concentrate to improve water recovery in wastewater reclamation, Journal of Membrane Science 378 (2011) 101–110. doi:10.1016/j.memsci.2010.10.036.
URL http://dx.doi.org/10.1016/j.memsci.2010.10.036

[16] M. Fidaleo, M. Moresi, Electrodialysis applications in the food industry, Advances in Food and Nutrition Research 51 (2006) 265–360. doi:10.1016/S1043-4526(06)51005-8.
URL http://dx.doi.org/10.1016/S1043-4526(06)51005-8

[17] K. M. Chehayeb, D. M. Farhat, K. G. Nayar, J. H. Lienhard V, Optimal design and operation of electrodialysis for brackish-water desalination and for high-salinity brine concentration, Desalination 420 (2017) 167 – 182. doi:https://doi.org/10.1016/j.desal.2017.07.003.
URL http://www.sciencedirect.com/science/article/pii/S0011916417305763

[18] D. Tondeur, E. Kvaalen, Equipartition of entropy production. An optimality criterion for transfer and separation processes, Industrial & Engineering Chemistry Research 26 (1) (1987) 50–56.

[19] R. K. McGovern, G. P. Thiel, G. P. Narayan, S. M. Zubair, J. H. Lienhard V, Performance limits of zero and single extraction humidification-dehumidification desalination systems, Applied Energy 102 (2013) 1081 – 1090. doi:http://dx.doi.org/10.1016/j.apenergy.2012.06.025.
URL http://www.sciencedirect.com/science/article/pii/S0306261912004709

[20] G. P. Narayan, K. M. Chehayeb, R. K. McGovern, G. P. Thiel, S. M. Zubair, J. H. Lienhard V, Thermodynamic balancing of the humidification dehumidification desalination system by mass extraction and injection, International Journal of Heat and Mass Transfer 57 (2) (2013) 756 – 770. doi:http://dx.doi.org/10.1016/j.ijheatmasstransfer.2012.10.068.
URL http://www.sciencedirect.com/science/article/pii/S0017931012008344

[21] K. M. Chehayeb, G. Prakash Narayan, S. M. Zubair, J. H. Lienhard, Use of multiple extractions and injections to thermodynamically balance the humidification dehumidification desalination system, International Journal of Heat and Mass Transfer 68 (2014) 422–434. doi:10.1016/j.ijheatmasstransfer.2013.09.025.
URL http://doi.org/10.1016/j.ijheatmasstransfer.2013.09.025

[22] K. M. Chehayeb, G. P. Narayan, S. M. Zubair, J. H. Lienhard V, Thermodynamic balancing of a fixed-size two-stage humidification dehumidification desalination system, Desalination 369 (2015) 125 – 139. doi:http://dx.doi.org/10.1016/j.desal.2015.04.021.
URL http://www.sciencedirect.com/science/article/pii/S0011916415002660

[23] H. W. Chung, J. Swaminathan, D. M. Warsinger, J. H. Lienhard V, Multistage vacuum membrane distillation (MSVMD) systems for high salinity applications, Journal of Membrane Science 497 (2016) 128 – 141. doi:http://dx.doi.org/10.1016/j.memsci.2015.09.009.
URL http://www.sciencedirect.com/science/article/pii/S0376738815301733

[24] Q. J. Wei, R. K. McGovern, J. H. Lienhard V, Saving energy with an optimized two-stage reverse osmosis system, Environ. Sci.: Water Res. Technol. (2017) –doi:10.1039/C7EW00069C.
URL http://dx.doi.org/10.1039/C7EW00069C

[25] P. Tsiakis, L. G. Papageorgiou, Optimal design of an electrodialysis brackish water desalination plant, Desalination 173 (2005) 173–186. doi:10.1016/j.desal.2004.08.031.

[26] A. D. Ryabtsev, N. P. Kotsupalo, V. I. Titarenko, I. K. Igumenov, N. V. Gelfond, N. E. Fedotova, N. B. Morozova, V. A. Shipachev, A. S. Tibilov, Development of a two-stage electrodialysis set-up for economical desalination of sea-type artesian and surface waters, Desalination 137 (01) (2001) 207–214. doi:10.1016/S0011-9164(01)00220-X.

[27] Y. Tanaka, Ion-exchange membrane electrodialysis program and its application to multi-stage continuous saline water desalination, Desalination 301 (2012) 10 – 25. doi:http://dx.doi.org/10.1016/j.desal.2012.06.007.
URL http://www.sciencedirect.com/science/article/pii/S0011916412003153

[28] R. K. McGovern, S. M. Zubair, J. H. Lienhard V, Hybrid electrodialysis reverse osmosis system design and its optimization for treatment of highly saline brines, IDA Journal of Desalination and Water Reuse 6 (1) (2014) 15–23. doi:10.1179/2051645214Y.0000000016.
URL http://dx.doi.org/10.1179/2051645214Y.0000000016

[29] G. P. Thiel, R. K. McGovern, S. M. Zubair, J. H. Lienhard V, Thermodynamic equipartition for increased second law efficiency, Applied Energy 118 (2014) 292–299. doi:10.1016/j.apenergy.2013.12.033.
URL http://doi.org/10.1016/j.apenergy.2013.12.033

[30] K. M. Chehayeb, J. H. Lienhard V, Entropy generation analysis of electrodialysis, Desalination 413 (2017) 184–198. doi:10.1016/j.desal.2017.03.001.
URL http://dx.doi.org/10.1016/j.desal.2017.03.001

[31] E. Johannessen, L. Nummedal, S. Kjelstrup, Minimizing the entropy production in heat exchange, International Journal of Heat and Mass Transfer 45 (13) (2002) 2649 – 2654. doi:http://dx.doi.org/10.1016/S0017-9310(01)00362-3.
URL http://www.sciencedirect.com/science/article/pii/S0017931001003623

[32] E. Johannessen, S. Kjelstrup, A highway in state space for reactors with minimum entropy production, Chemical Engineering Science 60 (12) (2005) 3347 – 3361. doi:https://doi.org/10.1016/j.ces.2005.01.026.
URL http://www.sciencedirect.com/science/article/pii/S0009250905000862

[33] E. Magnanelli, E. Johannessen, S. Kjelstrup, Entropy production minimization as design principle for membrane systems: Comparing equipartition results to numerical optima, Industrial & Engineering Chemistry Research 56 (16) (2017) 4856–4866. doi:10.1021/acs.iecr.7b00493.
URL https://doi.org/10.1021/acs.iecr.7b00493

[34] H. B. Callen, Thermodynamics and an introduction to thermostatistics, John Wiley & Sons, 1985.

[35] A. Bejan, Advanced engineering thermodynamics, John Wiley & Sons, 2006.

[36] R. K. McGovern, A. M. Weiner, L. Sun, C. G. Chambers, S. M. Zubair, J. H. Lienhard V, On the cost of electrodialysis for the desalination of high salinity feeds, Applied Energy 136 (2014) 649–661. doi:10.1016/j.apenergy.2014.09.050.
URL http://dx.doi.org/10.1016/j.apenergy.2014.09.050

[37] M. Fidaleo, M. Moresi, Optimal strategy to model the electrodialytic recovery of a strong electrolyte, Journal of Membrane Science 260 (2005) 90–111. doi:10.1016/j.memsci.2005.01.048.
URL http://dx.doi.org/10.1016/j.memsci.2005.01.048

[38] G. Kraaijeveld, V. Sumberova, S. Kuindersma, H. Wesselingh, Modelling electrodialysis using the Maxwell-Stefan description, The Chemical Engineering Journal and the Biochemical Engineering Journal 57 (1995) 163–176. doi:10.1016/0923-0467(94)02940-7.
URL http://dx.doi.org/10.1016/0923-0467(94)02940-7

[39] O. Kuroda, S. Takahashi, M. Nomura, Characteristics of flow and mass transfer rate in an electrodialyzer compartment including spacer, Desalination 46 (1983) 225–232. doi:10.1016/0011-9164(83)87159-8.
URL http://dx.doi.org/10.1016/0011-9164(83)87159-8

[40] R. A. Robinson, R. H. Stokes, Electrolyte solutions, Courier Corporation, 2002.

[41] T. Shedlovsky, The electrolytic conductivity of some uni-univalent electrolytes in water at 25 C, Journal of the American Chemical Society 54 (1932) 1411–1428. doi:10.1021/ja01343a020.
URL http://dx.doi.org/10.1021/ja01343a020

[42] J. F. Chambers, J. M. Stokes, R. H. Stokes, Conductances of concentrated aqueous sodium and potassium chloride solutions at 25 C, The Journal of Physical Chemistry 60 (1956) 985–986. doi:10.1021/j150541a040.
URL http://dx.doi.org/10.1021/j150541a040

[43] K. M. Chehayeb, Thermodynamic analysis of electrodialysis, Ph.D. thesis, Massachusetts Institute of Technology (2017).

[44] G. Kraaijeveld, The Maxwell-Stefan description of mass transfer in ion exchange and electrodialysis, Ph.D. thesis, University of Groningen (1994).

[45] K. G. Nayar, M. H. Sharqawy, L. D. Banchik, J. H. Lienhard V, Thermophysical properties of seawater: A review and new correlations that include pressure dependence, Desalination 390 (2016) 1 – 24. doi:10.1016/j.desal.2016.02.024.
URL http://dx.doi.org/10.1016/j.desal.2016.02.024

[46] K. G. Nayar, G. P. Thiel, M. H. Sharqawy, J. H. Lienhard V, Seawater flow exergy calculations and the minimum energy for seawater desalination: An update, Desalination (Manuscript in preparation).

[47] G. P. Thiel, E. W. Tow, L. D. Banchik, H. W. Chung, J. H. Lienhard V, Energy consumption in desalinating produced water from shale oil and gas extraction, Desalination 366 (2015) 94 – 112. doi:10.1016/j.desal.2014.12.038.
URL http://dx.doi.org/10.1016/j.desal.2014.12.038

[48] G. P. Thiel, J. H. Lienhard V, Treating produced water from hydraulic fracturing: Composition effects on scale formation and desalination system selection, Desalination 346 (2014) 54 – 69. doi:10.1016/j.desal.2014.05.001.
URL http://dx.doi.org/10.1016/j.desal.2014.05.001

[49] K. S. Pitzer, J. J. Kim, Thermodynamics of electrolytes. IV. Activity and osmotic coefficients for mixed electrolytes, Journal of the American Chemical Society 96 (1974) 5701–5707. doi:10.1021/ja00825a004.
URL http://dx.doi.org/10.1021/ja00825a004

[50] K. S. Pitzer, A thermodynamic model for aqueous solutions of liquid-like density, Reviews in Mineralogy and Geochemistry 17 (1987) 97–142.

[51] C. E. Harvie, J. H. Weare, The prediction of mineral solubilities in natural waters: the Na-K-Mg-Ca-Cl-SO_4-H_2O system from zero to high concentration at 25 C, Geochimica et Cosmochimica Acta 44 (1980) 981 – 997. doi:10.1016/0016-7037(80)90287-2.
URL http://dx.doi.org/10.1016/0016-7037(80)90287-2

[52] C. E. Harvie, N. Møller, J. H. Weare, The prediction of mineral solubilities in natural waters: The Na-K-Mg-Ca-H-Cl-SO_4-OH-HCO_3-CO_3-CO_2-H_2O system to high ionic strengths at 25 C, Geochimica et Cosmochimica Acta 48 (1984) 723–751. doi:10.1016/0016-7037(84)90098-X.
URL http://dx.doi.org/10.1016/0016-7037(84)90098-X

[53] K. S. Pitzer, Thermodynamics of electrolytes. I. Theoretical basis and general equations, The Journal of Physical Chemistry 77 (1973) 268–277. doi:10.1021/j100621a026.
URL http://dx.doi.org/10.1021/j100621a026

[54] K. S. Pitzer, J. C. Peiper, R. Busey, Thermodynamic properties of aqueous sodium chloride solutions, Journal of Physical and Chemical Reference Data 13 (1984) 1–102. doi:10.1063/1.555709.
URL http://dx.doi.org/10.1063/1.555709

[55] T. W. Chapman, Transport properties of concentrated electrolytic solutions, Ph.D. thesis, University of California, Berkeley (1967).

[56] R. Mills, V. M. Lobo, Self-diffusion in electrolyte solutions, Elsevier Science, Amsterdam, Netherlands, 1989.

List of Figures